iREVIEWS

STATE-OF-THE-ART PAPERS

New Applications of Cardiac Computed Tomography

Dual-Energy, Spectral, and Molecular CT Imaging

CrossMark

Ibrahim Danad, MD,* Zahi A. Fayad, PhD,† Martin J. Willemink, MD,†‡ James K. Min, MD*

ABSTRACT

Computed tomography (CT) has evolved into a powerful diagnostic tool, and it is impossible to imagine current clinical practice without CT imaging. Because of its widespread availability, ease of clinical application, superb sensitivity for the detection of coronary artery disease, and noninvasive nature, CT has become a valuable tool within the armamentarium of cardiologists. In the past few years, numerous technological advances in CT have occurred, including dual-energy CT, spectral CT, and CT-based molecular imaging. By harnessing the advances in technology, cardiac CT has advanced beyond the mere evaluation of coronary stenosis to an imaging tool that permits accurate plaque characterization, assessment of myocardial perfusion, and even probing of molecular processes that are involved in coronary atherosclerosis. Novel innovations in CT contrast agents and pre-clinical spectral CT devices have paved the way for CT-based molecular imaging. (J Am Coll Cardiol Img 2015;8:710–23) © 2015 by the American College of Cardiology Foundation.

Since the advent of 64-detector row computed tomography (CT) in 2005, coronary computed tomographic angiography (CTA) has been demonstrated as a promising noninvasive technique for the evaluation of coronary artery stenosis (1,2). In the past few years, numerous technological advances in CT have occurred, including dual-energy computed tomography (DECT), spectral CT, and CT-based molecular imaging. Early studies of these methods have been largely promising and shown improved cardiac and coronary evaluation. An understanding of these advanced CT principles is required to fully appreciate the promise of the applicability of these technologies for the evaluation of patients with cardiac and coronary disease.

THE PRINCIPLES OF DECT

Improvements in CT, although rapid in recent years, are nevertheless constrained by the physical principles underlying this technology, which are a function of x-ray attenuation detected from multiple orientations around an imaged object. In a basic sense, these principles are generally 2-fold and include the photoelectric and Compton effects when considering x-ray photons within the diagnostic energy range

(Figure 1). The former is highly dependent on the photon energy level and is related to the atomic number and photon energy level, whereas the latter is independent of the photon energy level but rather related to material density. For a proper grasp of the advances in DECT and spectral CT, a basic understanding of these principles is required.

The photoelectric effect is the ejection of an electron from the innermost shell of an atom (the K shell) by a photon with a greater energy than the binding energy of the K shell. As a result, the total energy of any incoming photon is absorbed (Figure 1). The binding energy of electrons in the K shell is material specific and is proportional to the atomic number (Z). For a given photon energy, the photoelectric effect scales on a magnitude order of Z^3. However, this does not imply that an element with $Z = 100$ yields an 8 times greater attenuation than a material with $Z = 50$. This can be explained by the spike in attenuation seen related to a maximal photoelectric effect (the K edge), which occurs when the photon energy level is just greater than the electron binding energy of the K shell of an atom. The K-edge value varies for each material and is higher with increasing atomic numbers. Paradoxically, the photoelectric effect is maximal at the K edge of the absorber and is reduced with increasing photon energy levels, inversely proportional to the photon energy cubed ($1/E^3$). Therefore, the probability of the photoelectric effect is dependent on both the atomic number and the photon energy level according to Z^3/E^3.

The Compton effect is the collision of photons with valence electrons of the outermost shell of an atom. In contrast to the photoelectric effect, the energy of the incoming photon is not totally absorbed, giving rise to photon scattering (Figure 1). Compton scattering is dependent on the density of electrons, and because all elements have approximately the same amount of electrons per unit mass, the atomic number is of less relevance for the occurrence of Compton scattering.

The principles of DECT are based largely on the photoelectric effect and can be achieved by exploiting the energy-dependent attenuation of materials when exposed to 2 different photon energy levels. These physical principles can be exploited for in vivo human imaging, because DECT is based on dissimilar tissue characteristics with respect to their energy-dependent x-ray attenuation. Subsequently, DECT enables the distinct differentiation between 2 basis materials (Figure 2). These materials can be chosen arbitrarily, as long as their K edges are sufficiently different (i.e., attenuation profiles), such as water and iodine. Any other material with an attenuation

spectrum different than that of the chosen basis materials will be reflected as a combination of the 2 basis materials (Figure 3). As such, by exploiting differences in energy-related attenuation of tissues, DECT provides information about tissue composition that is unobtainable with conventional single-energy computed tomography (SECT).

The advantage of using different energy x-ray levels for decomposition of tissues has been known for a long time and was even mentioned by Hounsfield (3) in his original paper on CT 4 decades ago: "Two pictures are taken of the same slice, one at 100 kV and the other at 140 kV so that areas of high atomic numbers can be enhanced. Tests carried out to date have shown that iodine (Z = 53) can be readily distinguished from calcium (Z = 20)". However, this approach at that time was subject to technological limitations and was therefore abandoned.

DECT METHODS

Although SECT is typically performed with polychromatic energy levels of photons set to 120 or 140 kVp, energy levels of photons with DECT are typically 80 and 140 kVp for the acquisition of low- and high-energy-dependent tissue attenuation profiles, respectively. The exploitation of 2 polychromatic energy spectra by DECT can be achieved by at least 3 different methods (Figure 4): 1) 2 x-ray source and detector pairs, with each source operating at a different tube voltage; 2) a single source-detector pair with an x-ray tube capable of rapidly switching between low and high tube potential or by switching tube potential between gantry positions; and 3) an x-ray source operating at constant tube voltage with a double-layer detector capable of differentiating between low- and high-energy photons.

CLINICAL APPLICATIONS OF DECT

MYOCARDIAL PERFUSION IMAGING. Compared with SECT, DECT may allow better tissue characterization and therefore enhanced visualization of myocardial perfusion defects, thus encouraging its use for ischemia assessment. Given the unique ability of DECT to allow differentiation of iodine attenuation characteristics when it is exposed to different photon energy levels, DECT allows the mapping of iodine distribution in the myocardium as a quantitative, albeit surrogate, marker for perfusion and blood volume (4) (Figure 5). There is an early body of evidence showing the clinical feasibility of a DECT myocardial

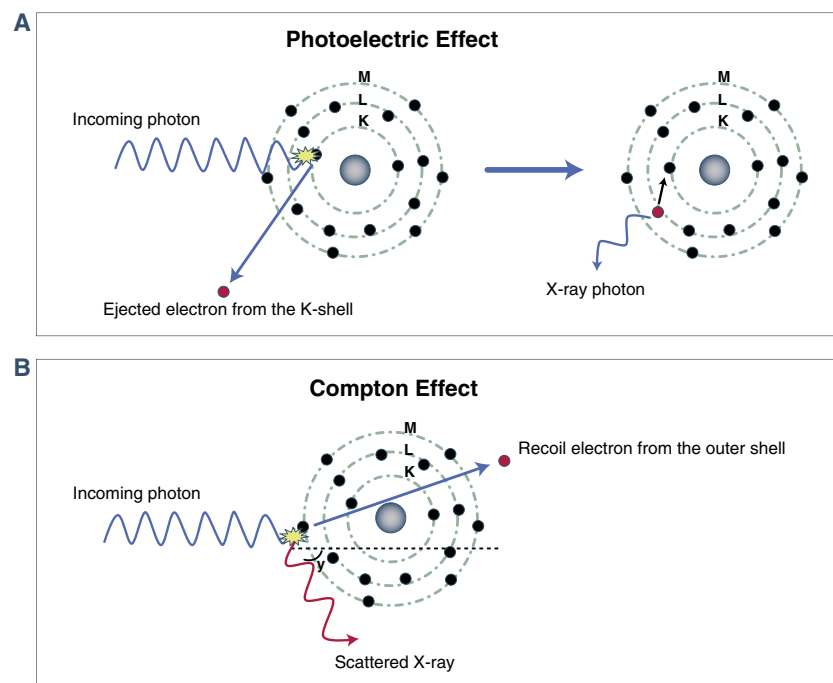perfusion protocol as a supplement to anatomic evaluation of the coronary arteries with coronary CTA (5-7). The majority of these investigations have compared DECT with rest-stress single-photon emission computed tomography (SPECT), cardiac magnetic resonance, or invasive coronary angiography as a reference standard (5,7-11). In a small study (n = 20) by Weininger et al. (12), stress-rest first-pass myocardial perfusion DECT detected myocardial perfusion defects on cardiac magnetic resonance with sensitivity and specificity of 93% and 99%, respectively. Also against a cardiac magnetic resonance reference standard, Ko et al. (9) found that stress-rest first-pass myocardial perfusion DECT could detect reversible perfusion defects with sensitivity and specificity of 89% and 78%, respectively. Although first-pass myocardial perfusion DECT alone revealed the diagnosis of ischemia corresponding to a ≥50% stenosis on invasive coronary angiography with sensitivity of 89% and specificity of 76% (9), it is conjectured that a hybrid approach—namely, combining DECT perfusion with coronary CTA—may

enhance the diagnostic accuracy of physiologic coronary artery disease assessment through improvements in specificity (13).

In this regard, 3 studies have demonstrated the incremental diagnostic value of combining DECT myocardial perfusion imaging (MPI) with coronary CTA (6,10). Ko et al. (6) showed that the addition of DECT perfusion to coronary CTA resulted in improvements in sensitivity, specificity, negative predictive value, and positive predictive value from 91.8%, 67.7%, 87.7%, and 73.6% to 93.2%, 85.5%, 91.4%, and 88.3%, respectively. Although Wang et al. (10) found no differences in sensitivity and negative predictive value (both remained at 100%), they reported specificity to significantly improve from 37.5% to 75.0% by the combination of DECT perfusion imaging with coronary CTA. A recently published study confirmed the incremental value of DECT perfusion imaging as an adjunct to coronary CTA, which decreased the number of false-positive results on coronary CTA, as reflected by improvements in both specificity and positive predictive value, from

FIGURE 1 Schematic Illustration of the Photoelectric and Compton Effects

A Photoelectric Effect

Incoming photon

Ejected electron from the K-shell

X-ray photon

B Compton Effect

Incoming photon

Recoil electron from the outer shell

Scattered X-ray

(A) Photoelectric effect: An incoming photon collides with an electron, and its energy is totally absorbed. If the kinetic energy of the photon is greater than the binding energy of the electron, this will result in its ejection out of the K shell (the innermost shell of an atom). An electron from another layer moves to occupy the vacancy left in the inner layer by the ejected electron. This transition is accompanied by the release of x-ray photons. **(B)** Compton effect: This is a radiation-scattering event, whereby the incoming x-ray photon ejects an electron from the outermost shell of an atom and is scattered. Because of its loss of kinetic energy, the wavelength of the incoming photon becomes longer, and the photon can become red shifted (red light has the longest wavelength).

56% to 79% and from 55% to 71%, respectively. As a consequence, the hybrid approach improved accuracy significantly from 69% to 82% (14).

These results suggest that MPI with DECT may decrease the number of false-positive results on coronary CTA, which is in line with the observations seen for hybrid positron emission tomography and SPECT and coronary CTA (15). Despite the notion that combined physiologic-anatomic evaluation by DECT provided additive diagnostic value, Wang et al. (5) observed a negligible effect of MPI with DECT when added to coronary CTA for measures of diagnostic accuracy, with a compromised increase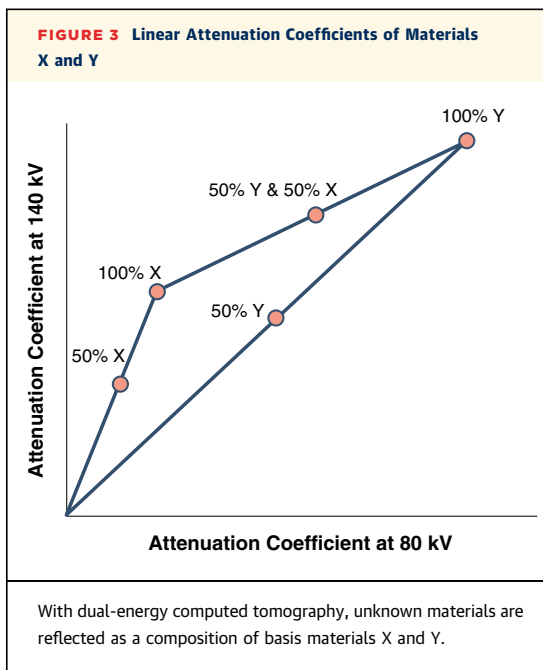 in sensitivity from 82% to 90% at the loss of specificity (from 91% to 86%). Similarly, a recently published pilot study reported MPI with DECT to improve the accuracy of coronary CTA alone, but the combination of these 2 tests resulted in lower performance compared with DECT perfusion imaging alone (16).
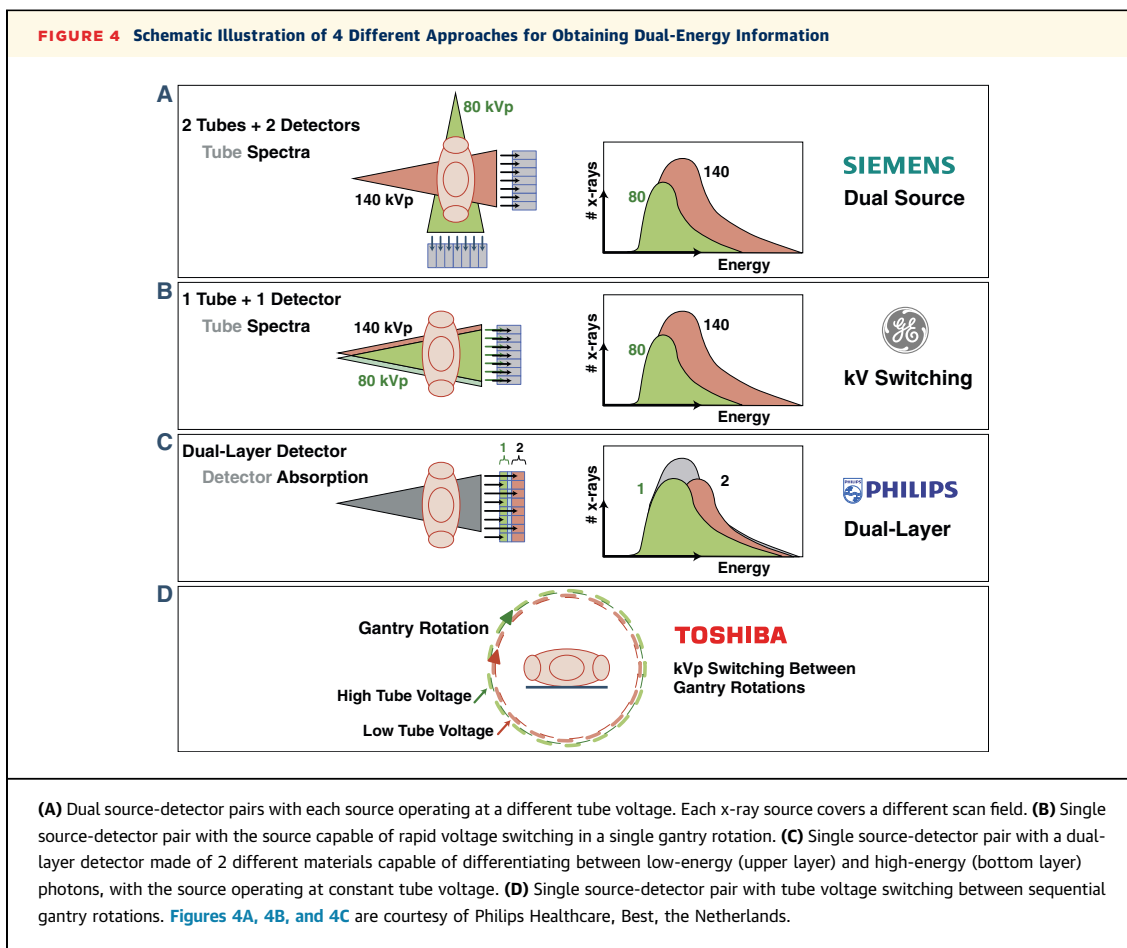
Several important considerations of MPI with DECT have been discussed and require attention for the optimization of MPI protocols. Among the early studies of MPI with DECT, there has been variability regarding when to perform the "rest" portion and the "stress" portion, with many contending that vasodilator stress is important to perform first to reduce the chance of residual contrast that may confound perfusion defects. Others have argued for a rest-first protocol, maintaining the importance of coronary artery evaluation by coronary CTA as the foremost information to be garnered from the study. Pertaining to the latter, rest DECT has been reported to allow the detection of perfusion defects not visible on rest SPECT (5,11), suggesting its use as a possible adjunct to traditional evaluation with coronary CTA. This finding may be due to myriad reasons, including the higher spatial resolution of CT, which may encourage the detection of subtle perfusion abnormalities that are not visible on SPECT (5,11,17). However, a recent study by Ko et al. (14) reported stress MPI with DECT to convey higher accuracy for the detection of ischemia compared with rest DECT perfusion imaging. Despite these early studies emphasizing the potential of DECT to provide complementary information on coronary artery disease, MPI with DECT may be regarded as being in its infancy, with published studies to date limited by small sample sizes, referral bias, and the lack of a proper reference standard.

CORONARY ATHEROSCLEROTIC PLAQUE CHARACTERIZATION. From prior invasive and pathologic evaluations, several coronary atherosclerotic plaque features have been implicated as crucial to the pathogenesis of acute coronary syndromes, including

FIGURE 2 Mass Attenuation Coefficients for Iodine, Calcium, and Water at Different Photon Energies

Note the attenuation peak of iodine ($Z = 53$) at 33 keV. This peak represents the K edge of iodine.
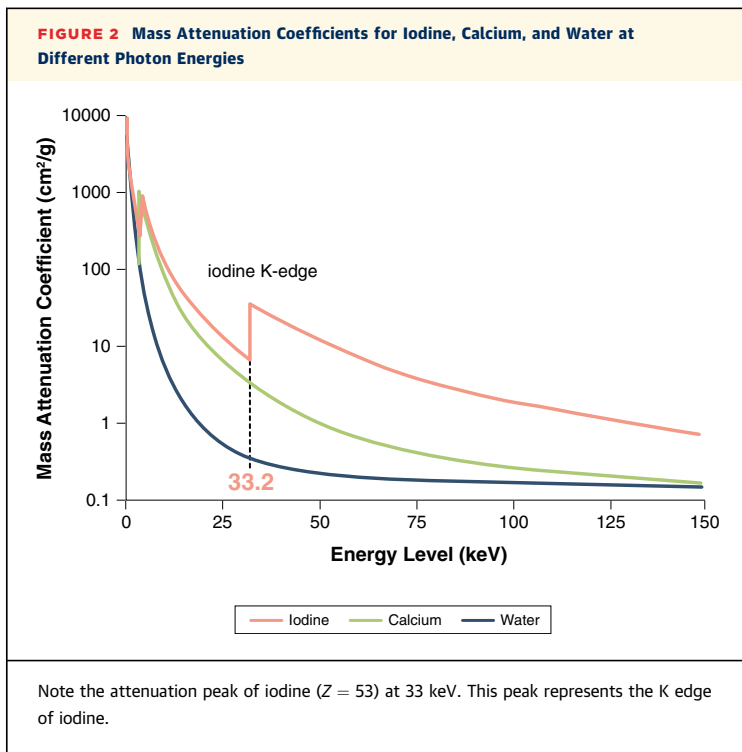
measures of plaque burden, thin-cap fibroatheroma, inflammatory infiltration, intraplaque hemorrhage, microcalcifications, and a necrotic lipid-rich core (18-20). Considering their importance, these plaque features have been extensively investigated by SECT, given the relative ease with which SECT can reliably

FIGURE 3 Linear Attenuation Coefficients of Materials X and Y

With dual-energy computed tomography, unknown materials are reflected as a composition of basis materials X and Y.

FIGURE 4 Schematic Illustration of 4 Different Approaches for Obtaining Dual-Energy Information

(A) Dual source-detector pairs with each source operating at a different tube voltage. Each x-ray source covers a different scan field. **(B)** Single source-detector pair with the source capable of rapid voltage switching in a single gantry rotation. **(C)** Single source-detector pair with a dual-layer detector made of 2 different materials capable of differentiating between low-energy (upper layer) and high-energy (bottom layer) photons, with the source operating at constant tube voltage. **(D)** Single source-detector pair with tube voltage switching between sequential gantry rotations. **Figures 4A, 4B, and 4C** are courtesy of Philips Healthcare, Best, the Netherlands.

separate calcified and noncalcified plaques. Yet, conventional CT faces a significant challenge in differentiating different components of noncalcified plaques (e.g., lipid-rich vs. fibrous). Several studies have shown considerable overlap in Hounsfield units between lipid-rich and fibrous-rich noncalcified plaques inherent to the spatial resolution of CT and a variable intraplaque uptake of iodine contrast agents (21–23).

It has been posited that DECT may overcome these limitations because of its capability for tissue decomposition, although early results have been mixed. CT attenuation-based characterization of noncalcified plaques using DECT was examined in an ex vivo study of 15 human arteries, with discriminatory improvement with DECT over conventional SECT (24). In contrast, in a small prospective study of patients undergoing intravascular ultrasound and CT, DECT had similar sensitivity compared with SECT (45% vs. 39%, respectively) for necrotic core detection (25). Even when using post-mortem samples, in which image quality is not governed by body

habitus or motion, DECT misclassified 21% of non-calcified plaques (26).

The mixed findings observed to date may be due to an array of issues, including scanning protocols as well as DECT image visualization. As indicated earlier, DECT may allow both monochromatic energy imaging as well as material basis decomposition. To date, the exact energy and/or material basis pair that optimizes plaque visualization has not been systematically evaluated. Future studies will be required to determine the proper methods for plaque characterization by this emerging technology.

MINIMIZING IMAGE ARTIFACTS USING DUAL-ENERGY COMPUTED TOMOGRAPHY

Image quality is particularly challenging when it comes to a moving organ such as the heart. Sufficient diagnostic image quality is highly dependent on the patient's heart rate. Therefore, heart rate control is mandatory when performing CT-based coronary angiography. Alternatively, dual-source CT is less

FIGURE 5   **A 77-Year-Old Woman With Hypertension, Hypercholesterolemia, and Atypical Angina Chest Pain**
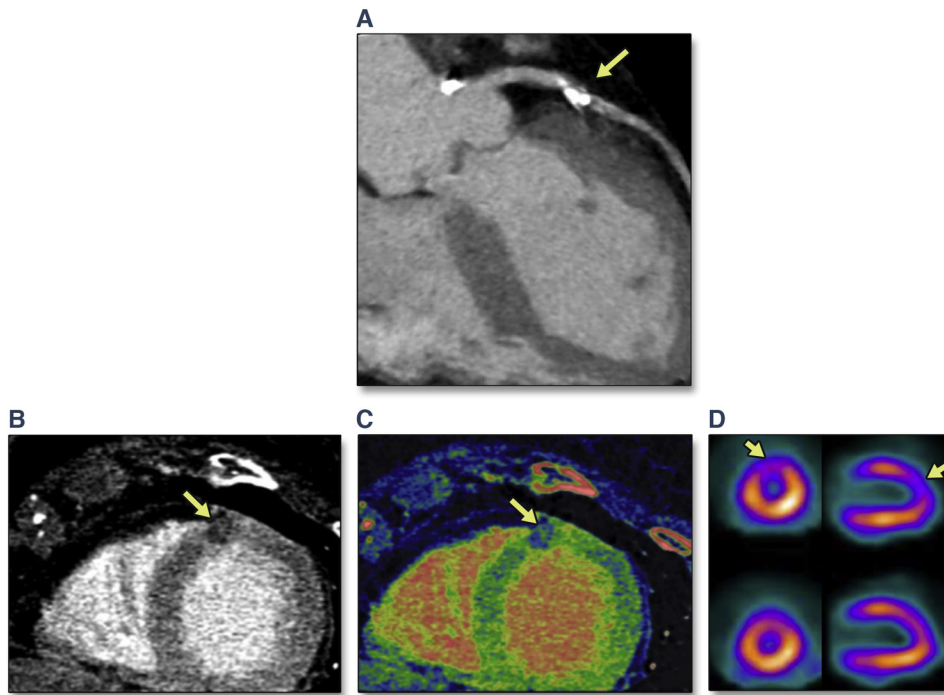
(A) Curved multiplanar reformatting of the left anterior descending coronary artery shows a calcified plaque with significant stenosis. **(B to D)** Assessment of computed tomographic perfusion **(B)** and myocardial blood flow map **(C)** revealed an anterior perfusion defect **(arrows, B and C)**, which was confirmed by single-photon emission computed tomography **(arrows, D)**.

susceptible to artifacts as a result of high or irregular heart rates, because of its high temporal resolution. Scheffel et al. (27) demonstrated dual-source CT to provide high diagnostic accuracy for the detection of coronary artery disease in patients with extensive calcifications (50% had Agatston scores >400) and without heart rate control, a population that is often considered challenging for conventional coronary CTA. Additionally, in a recent meta-analysis, dual-source CT in patients with atrial fibrillation yielded similar diagnostic value as standard coronary CTA in patients with stable and regular heart rates (28). The improved performance of dual-source CT in this specific population is attributable to the high temporal resolution of dual-source CT (66 to 75 ms), which allows fewer motion artifacts to occur (28). Furthermore, the unique features of the DECT dataset allows the generation of virtual monochromatic images, which are analogous to conventional single-energy CT images. However, monochromatic images depict a scanned object at a single x-ray energy level, rendering these images less susceptible to beam-hardening and blooming artifacts (29–31).

Because of the polychromatic nature of the x-rays used in conventional CT, imaging of high-density objects will result in substantial absorption of lower energy photons, giving rise to a shift towards a high-energy x-ray beam. This alteration of the photon-energy spectrum leads to distortions in the reconstructed image of high-attenuation tissue or objects, such as, among others, coronary stents, highly concentrated contrast, and/or calcium. Indeed, coronary calcifications and metal artifacts from coronary stents are known for hampering the diagnostic value of CT-based coronary artery imaging. Interestingly, monochromatic images at high energy levels suffer less from blooming and beam-hardening artifacts. Therefore, analyzing monoenergetic high-energy images carries with it the potential to reduce these artifacts (32). It has been demonstrated that calcium blooming and beam-hardening artifacts that impair accurate delineation of stenosis degree are significantly reduced at high energy levels using phantom models (33,34). Another phantom study showed improved enhancement of coronary stent lumen, beyond that achieved with traditional CT,

using DECT technology based on a dual-layer detector (33). A recently published feasibility study performed in 21 patients revealed that single-source DECT (with rapid tube voltage switching) with monochromatic image reconstructions below 80 keV was associated with an increase in stent-related blooming artifacts, causing an underestimation of stent diameter (35). Similarly, Secchi et al. (36) evaluated artifact size in 35 patients and reported substantial reductions of high-attenuation artifacts, resulting from metal artifacts (coronary stents, bypass clips, and sternal wires) and concentrated contrast in the vena cava, by using monochromatic images at high energy levels. With stress myocardial perfusion CT, beam hardening arising from high-density iodinated contrast hampers accurate assessment of myocardial perfusion. Studies using ex vivo hearts and phantom models demonstrated improved detection of myocardial perfusion defects by reduction of beam-hardening artifacts mimicking perfusion deficits using fast-switching tube voltage DECT technology (37,38). A clinical study by So et al. (4) showed rapid tube voltage-switching projection-based DECT to improve ischemia detection by the elimination of beam-hardening artifacts. Notably, DECT data obtained with a rapid tube voltage-switching DECT device allows the generation of monochromatic images from projection space, theoretically providing a more sophisticated beam-hardening correction over the image-based method (38-40). However, clinical studies on this topic are currently lacking.

RADIATION DOSE ASPECTS OF DECT

Although cardiac CT provides invaluable information regarding diagnosis and the management of patients evaluated for coronary artery disease, the exposure to ionizing radiation is of concern with CT-based imaging. In recent years, substantial reductions in radiation dose have been achieved with the implementation of electrocardiographically guided tube modulation, prospective electrocardiographically gated imaging (step-and-shoot mode), and body mass index–based tube voltage reductions. As a consequence, dose reductions of more than 60%, and even 90% in some studies, have been achieved without sacrifices in image quality and diagnostic performance (41-44). Nevertheless, the question arises of whether cardiac imaging using DECT comes with a radiation dose penalty compared with SECT. In an early small clinical study, dual-source CT in single-energy mode (4.54 ± 1.87 mSv) and DECT (9.8 ± 4.77 mSv) were shown to deliver less radiation than regular 16-slice multidetector coronary CTA (12.00 ± 3.59 mSv)
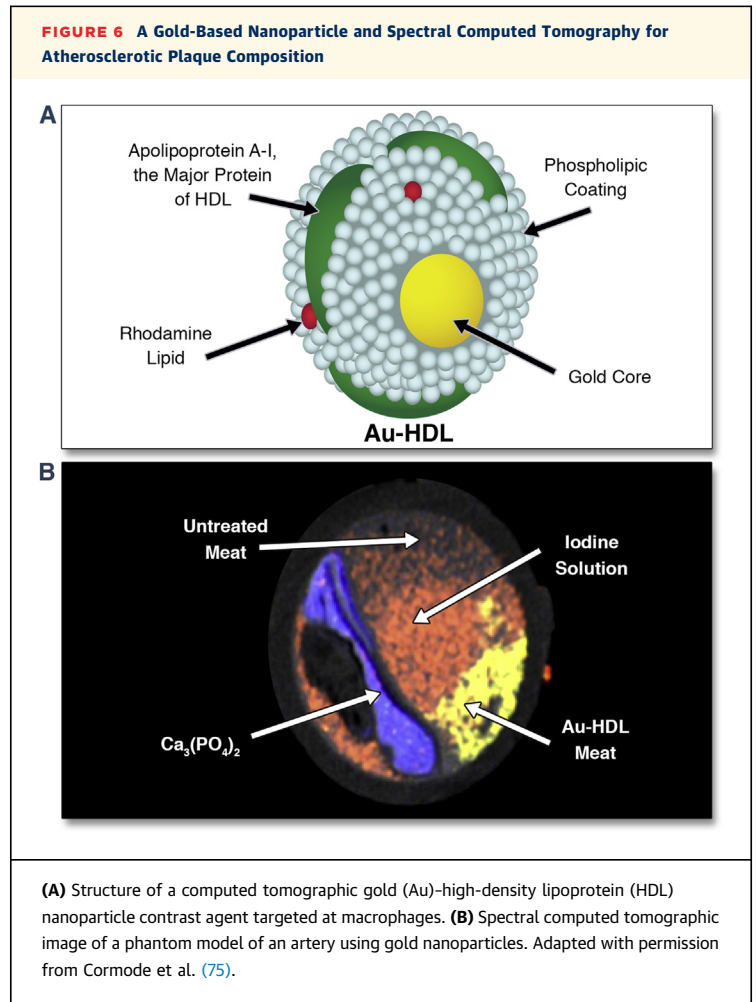
in a routine clinical setting in patients with low and stable heart rates (45). Halliburton et al. (46) compared in a clinical setting dual-source and 32-slice CT with regard to radiation exposure, and they showed no difference in radiation doses for coronary imaging between the 2 modalities. Similarly, in a head-to-head prospective randomized clinical trial evaluating 102 patients, DECT based on rapid tube voltage switching enabled coronary CTA examinations at dosage levels comparable with contemporary multidetector coronary CTA, 2.31 mSv versus 2.23 mSv, respectively (47). Although no study has evaluated the radiation dose of DECT devices on the basis of double-layer technology for cardiac imaging, presumably these devices will produce similar radiation doses overall to SECT, because there is no double irradiation of tissue to obtain low- and high-energy datasets. However, these data are acquired at 140 kVp, which is a high tube potential for most cardiac imaging. Arguably, lowering tube current will balance the effects of high-tube voltage imaging without affecting spectral separation, but data are so far lacking.

Radiation dose in cardiac CT is closely related to the pitch value, whereby a pitch value <1 implies overlapping image slices (table movement is less than 1 detector width during 1 gantry rotation) and a pitch >1 indicates gaps between radiation beams. Interestingly, dual-source CT systems have enabled the implementation of high-pitch spiral acquisition protocols with pitch values of 3.0 and higher, avoiding overlapping radiation exposure, allowing shorter scan times, and thus reducing effective radiation dose (48-50). Notably, high-pitch spiral acquisition is only possible with dual-source CT because of its unique geometry of a dual-source detector pair providing, among other features, high temporal resolution by using only a quarter of the gantry rotation time to obtain 1 cross-sectional image. The tube-detector pair allows fast table movement, whereby image gaps in the trajectory of the first detector are covered by the second detector. As such, the dual-source, high-pitch mode allows coverage of the entire heart in the diastolic phase of 1 cardiac cycle, which is referred to as prospective electrocardiographically gated spiral scanning. This approach has markedly reduced radiation doses to sub-millisievert fractions, albeit in single-energy mode (48-56). Clinical feasibility studies have investigated the diagnostic accuracy of high-pitch protocols and found that CT-based coronary angiography could be performed with effective radiation doses averaging 1 mSv, without a penalty in terms of diagnostic accuracy and image quality (48-56). Although high-pitch scanning holds great promise, a drawback of

this mode is that the image data of the entire heart need to be acquired during the diastasis of 1 heartbeat. Consequently, with the second-generation, dual-source devices (acquisition speed 458 mm/s and temporal resolution of 75 ms at a gantry rotation time of 282 ms), coverage of the entire heart (~12 cm) typically requires 250 ms. Therefore, the high-pitch mode is restricted to patients with low (<65 beats/min) and regular heart rates to match the required long image acquisition window (48-52,55). Recently, pilot studies demonstrated the feasibility of high-pitch coronary examinations using third-generation dual-source CT devices (acquisition speed 737 mm/s and temporal resolution of 66 ms owing to a gantry rotation time of 250 ms) to obtain good-quality images at heart rates up to 75 beats/min with submillisievert radiation dose (53,56).

Notably, the submillisievert radiation doses were achieved with a combination of multiple dose-saving strategies, such as prospective electrocardiographic triggering, low tube voltages, and iterative image reconstruction. The increased image noise resulting from low-voltage imaging is offset by the application of iterative reconstruction techniques (54,57,58). These novel reconstruction algorithms have reduced image noise derived from low-photon counting, while increasing image quality. A recently published small-scale clinical study of 26 patients revealed an effective radiation dose to be 0.3 mSv using a third-generation dual-source device capable of producing high tube current at a tube voltage of 70 kVp without a sacrifice in image quality, albeit in a population selected by body weight (<100 kg) with low heart rates (54). Similarly, Schuhbaeck et al. (57) managed to reduce effective radiation dose below 0.1 mSv in 21 patients using a high-pitch spiral acquisition mode with low tube voltage (80 kVp) in conjunction with low tube voltage and iterative image reconstruction. In addition, the diagnostic performance of submillisievert coronary CTA is high, using invasive coronary angiography as a reference, despite the low radiation dose delivered to patients (59). By harnessing the advantages of dual-source CT devices combined with low-voltage imaging and iterative image reconstructions, the radiation dose of a coronary CT study is only a fraction of 1 mSv, which is comparable with the dose of a mammogram (0.4 mSv).

Another application of DECT for further radiation dose reduction is the generation of virtual unenhanced (VUE) images through the use of post-imaging reconstructions that are unique to DECT. These VUE images are generated from contrast-enhanced scans by virtual iodine subtraction using 3-material decomposition algorithms and may replace

FIGURE 6 **A Gold-Based Nanoparticle and Spectral Computed Tomography for Atherosclerotic Plaque Composition**

(A) Structure of a computed tomographic gold (Au)–high-density lipoprotein (HDL) nanoparticle contrast agent targeted at macrophages. **(B)** Spectral computed tomographic image of a phantom model of an artery using gold nanoparticles. Adapted with permission from Cormode et al. (75).

true contrast-enhanced scans (60,61). Subsequently, coronary artery calcium (CAC) scoring and standard contrast coronary CTA can all be gleaned from a single scan, obviating the need for separate non-contrast CAC scoring CT. In this way, scan acquisition time, costs, and radiation to the patient may be decreased. Several studies have already demonstrated the feasibility of CAC scoring using VUE imaging by showing good agreement of the CAC score derived from VUE images with true noncontrast CAC-scoring scans. Yamada et al. (62) revealed that DECT coronary angiography using VUE technology for calcium scoring resulted in a 20% dose reduction compared with conventional coronary CTA with a prior separate noncontrast CAC scan, while in a recently published study, an average dose reduction of 51% was seen by replacing separate CAC-scoring scans by VUE imaging for quantification of coronary calcium deposits (63). Although promising, the technique is still in its infancy, and further validation and more sophisticated correction algorithms

FIGURE 7   Mass Attenuation Coefficients for Iodine, Gadolinium, Gold, and Bismuth at Different Photon Energies
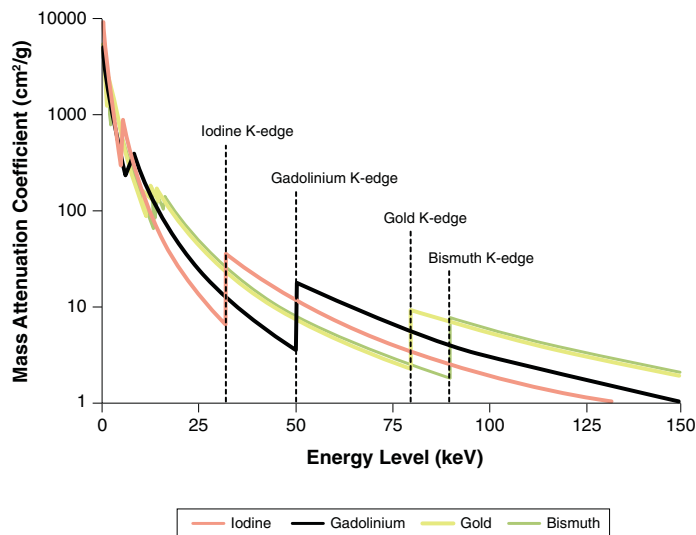
The lower energy photons of the spectrum are almost totally absorbed by surrounding tissues, rendering K-edge imaging using iodine contrast agents a challenging task.

are warranted to avoid underestimation of CAC burden by incorrect subtraction of calcium content–mimicking iodine contrast agents.
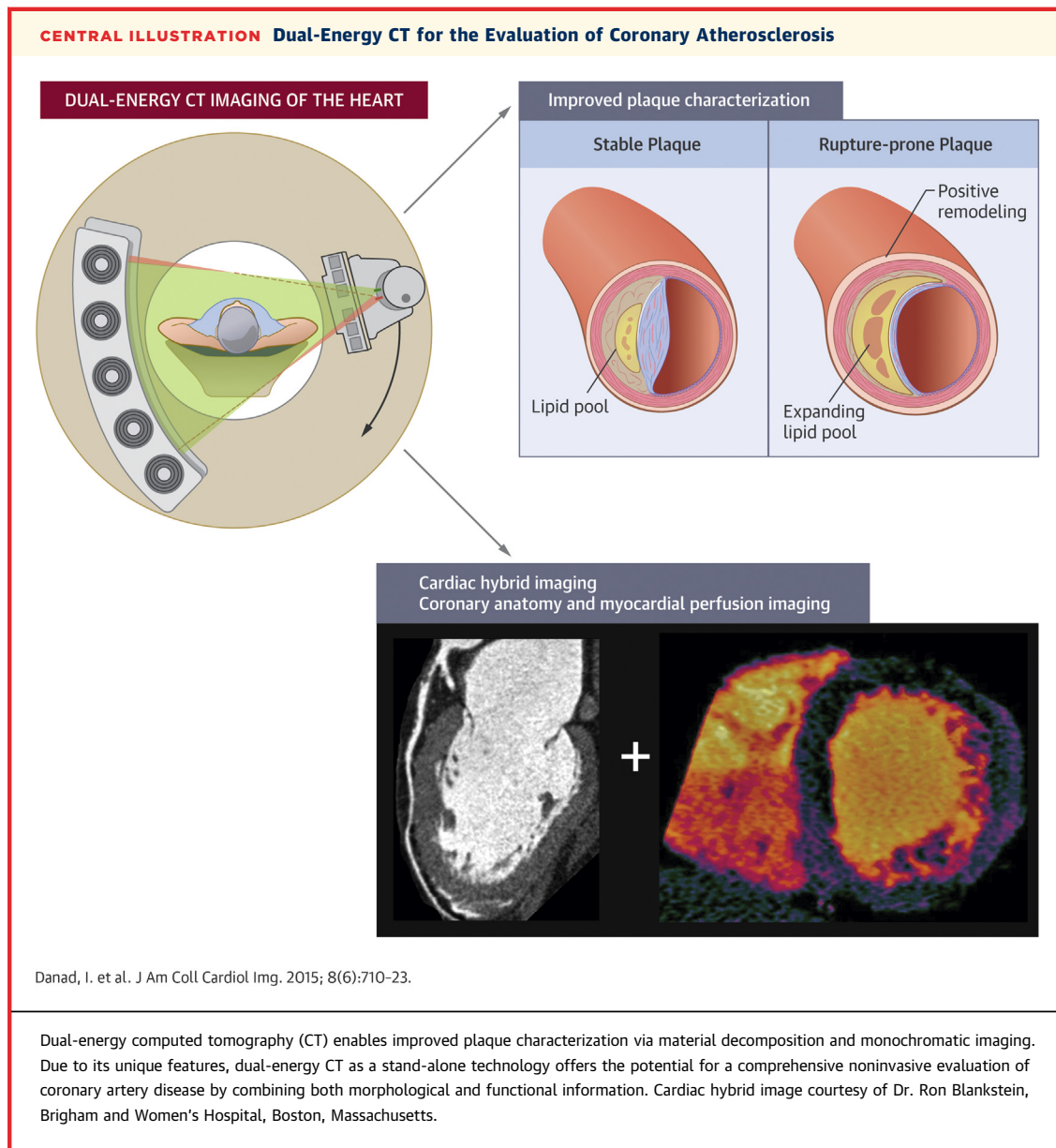
IODINATED CONTRAST DOSE REQUIREMENTS

Contrast-enhanced CT bears the risk of inducing an acute deterioration in renal function, particularly in patients with pre-existing kidney disease. Although the incidence of contrast-induced nephropathy is low, it is associated with significant morbidity and even death (64). However, lowering contrast volume comes at the cost of lower image quality due to impaired contrast-to-noise and signal-to-noise ratios (65). Nonetheless, previous studies have observed increased conspicuity of iodine-based contrast agents achieved with low tube voltage, while facilitating reductions in iodine load and radiation dose (30,66,67). In a recent study, Scheske et al. (29) reported improved signal-to-noise and contrast-to-noise ratios in both the myocardium and coronary arteries with low-energy monochromatic imaging compared with polychromatic CT. Therefore, an optimal difference in contrast attenuation between normally perfused myocardium (high attenuation) and ischemic myocardium is anticipated with low-energy monochromatic imaging, considering the low K edge of iodine. In a prospective randomized clinical study of 102 patients, Raju et al.

(47) evaluated the feasibility of DECT associated with reduced iodine load, and they found that monochromatic images at 60 keV provided signal- and contrast-to-noise ratios comparable to single-energy CT coronary angiography with a full iodine load, while preserving diagnostic interpretability. Interestingly, this was accomplished despite a more than 50% reduction in iodine load for CTA with DECT. Similarly, a recently published study revealed that monochromatic images at 50 to 60 keV allow an iodine volume reduction of up to 60% without compromising image quality, as reflected by similar contrast- and signal-to-noise ratios as those obtained with standard coronary CTA using a full iodine load (68).

COMPUTED TOMOGRAPHY–BASED MOLECULAR IMAGING: NANOPARTICLE CONTRAST AGENTS

Iodinated contrast and barium suspensions are currently the only approved CT contrast agents and are used for their ability to enhance visualization by increased attenuation of x-ray photons. Recently, nanoparticle contrast agents—tiny particles within the range of 1 to 100 nm—have received considerable attention (**Figure 6**). Several of these nanoparticles have been approved for therapeutic and diagnostic applications in the field of oncology (69,70). This is due to a number of reasons, including longer circulatory half-lives, obviating the need for repeated injections, and modifiable properties that offer tissue specificity (71-76).

One of the nanoparticle CT contrast agents with promising preliminary results is compound N1177. This is a suspension composed of crystalline iodinated particles dispersed with surfactant and has high affinity for activated macrophages (77). Upon injection, increased densities of N1177 contrast are detectable in atherosclerotic plaques that correspond to macrophage infiltration in post-mortem samples (77). Referenced against a histopathologic reference standard, N1177 demonstrates high affinity for aortic atherosclerosis in animal models and high correlation to fluorodeoxyglucose uptake, a known surrogate marker for macrophage density (78). In a related study by Cormode et al. (76), a gold-core high-density lipoprotein particle targeted at macrophages was found to accumulate in atherosclerotic plaques in the aorta walls of a mouse model as detected by micro-CT. Rabin et al. (79) developed a long circulating bismuth sulfide nanoparticle agent for CT. X-ray absorption was 5-fold better than with iodine, circulation times were longer than 2 h in vivo, and the efficacy and safety profiles were comparable with or

CENTRAL ILLUSTRATION Dual-Energy CT for the Evaluation of Coronary Atherosclerosis

DUAL-ENERGY CT IMAGING OF THE HEART

Improved plaque characterization

Stable Plaque | Rupture-prone Plaque

Positive remodeling

Lipid pool

Expanding lipid pool

Cardiac hybrid imaging
Coronary anatomy and myocardial perfusion imaging

Danad, I. et al. J Am Coll Cardiol Img. 2015; 8(6):710–23.

Dual-energy computed tomography (CT) enables improved plaque characterization via material decomposition and monochromatic imaging. Due to its unique features, dual-energy CT as a stand-alone technology offers the potential for a comprehensive noninvasive evaluation of coronary artery disease by combining both morphological and functional information. Cardiac hybrid image courtesy of Dr. Ron Blankstein, Brigham and Women's Hospital, Boston, Massachusetts.

better than those of iodinated contrast agents. Pan et al. (80) evaluated another heavy metal, ytterbium, for its use in spectral CT imaging. The specific goal of these particles would be the detection of nonocclusive microthrombus-associated ruptured plaques within the coronary arteries. It is notable to mention, however, that these encouraging findings have been validated in animal studies alone, with human evaluation currently lacking.

SPECTRAL CT IMAGING

Similar to DECT, spectral CT, often referred to as "multicolor CT," exploits the energy-dependent attenuation of x-ray photons and may be coupled to nanoparticles to potentially offer improved atherosclerosis evaluation. In contrast to DECT, which is performed with only 2 photon energy levels, spectral CT uses multiple energy levels to provide more detailed tissue information based on their behavior at different x-ray spectra (information that is disguised by the use of only 2 x-ray spectra). The principle of spectral CT relies on an energy-sensitive photon-counting detector that enables the differentiation of photons from multiple energy levels. In this configuration, when a photon collides with an x-ray detector, a current pulse is generated proportional to the energy of the detected x-ray photon.

Subsequently, the detected photon is allocated to energy bins representing several electron voltage intervals. A specific element can be more easily detected with the limits of the bins placed at the K edge of the material of interest. As such, simultaneous sampling of multiple photon energy levels allows a more sophisticated characterization of tissues on the basis of the K-edge behavior of multiple materials. To date, only pre-clinical data based on phantom models and post-mortem samples are available on coronary plaque imaging using photon-counting CT devices. Nevertheless, this technique holds great potential, allowing the precise detection and quantification of contrast agents and enabling their extraction and separation from tissue components (81). Different approaches for spectral CT are being developed. One of those is the Medipix All Resolution System CT scanner (CERN, Geneva, Switzerland), which incorporates a Medipix All Resolution System camera with a Medipix3 spectroscopic photon-counting detector (82). A single polychromatic x-ray tube is used in this system with an energy-discriminating photon-counting detector with selectable thresholds (83). So far, these scanners have been used in the pre-clinical setting. DxRay (DxRay Inc., Northridge, California) developed another photon-counting detector that was evaluated on a LightSpeed VCT scanner (GE Healthcare, Waukesha, Wisconsin). This detector is based on cadmium telluride and cadmium zinc telluride arrays (84). In vivo patient CT images were acquired, and the spectral technique was used to remove calcium from the images, resulting in a good image quality (84). Siemens Healthcare (Erlangen, Germany) developed another approach, a prototype scanner with a photon-counting technique implemented in the context of a clinical CT system (85). This prototype system is equipped with both a cadmium telluride photon-counting detector and a conventional detector from a clinical CT scanner. Using both approaches allows direct comparison of image quality between photon-counting and conventional detectors. A chess-pattern configuration for energy level thresholds enables a virtual number of 4 energy bins. Image acquisition of an anatomical phantom demonstrated increased iodine contrast, allowing a potential radiation dose reduction of up to 32%. Finally, Philips Medical Systems (Best, the Netherlands) developed a pre-clinical spectral CT scanner (86). This animal CT system is equipped with a single-line photon-counting cadmium telluride array that allows measurements of 6 energy bins (87). Feuerlein et al. (87) reported that this pre-clinical spectral CT system improved coronary luminal depiction by effectively isolating gadolinium agents from contrast-free calcified plaques and stent material using a phantom model. A recently published study by Boussel et al. (88) is the first study, albeit in vitro, of human coronary plaque analysis with the pre-clinical photon-counting spectral CT system. They reported promising results regarding its capability to differentiate distinct coronary plaque components on the basis of differences in spectral attenuation and iodine-based contrast concentrations. Of note, the absorption of low-energy photons by the human body renders the use of K-edge imaging with iodine challenging given its low K-edge energy of 33.2 keV. Therefore, to harness the full benefits of K-edge imaging using photon-counting CT, contrast materials with higher K edges, such as gadolinium (50.2 keV), gold (80.6 keV), and bismuth (90.5 keV), are preferable (**Figure 7**). However, the potential toxicity of these agents limits their use in humans. Nevertheless, the potential application of gold-based targeted nanoparticles in combination with spectral CT to improve tissue differentiation at the cellular level, albeit in phantom and animal models, has been explored. In a phantom study, Cormode et al. (75) demonstrated the feasibility and accuracy of the pre-clinical spectral CT scanner to simultaneously distinguish among iodine- and gold-based contrast agents, tissue, and calcifications. In addition, the investigators showed in an animal model the potential of this pre-clinical spectral CT system for imaging intraplaque inflammation using gold-labeled high-density lipoproteins targeting activated macrophages (75). These preliminary results illustrate the potential of CT-based molecular imaging using spectral CT in conjunction with nanoparticle contrast agents to provide valuable information on coronary atherosclerosis anatomy while providing important physiologic data at the molecular and cellular levels.

CONCLUSIONS

In recent years, there have been rapid advances in cardiac CT technology, with progression of conventional SECT to DECT, spectral CT, and CT-based molecular imaging. Initial studies of these technologies have been promising and suggest their potential for improved cardiac and coronary atherosclerosis evaluation (**Central Illustration**).

REPRINT REQUESTS AND CORRESPONDENCE: Dr. James K. Min, Weill Cornell Medical College, New York-Presbyterian Hospital, Dalio Institute of Cardiovascular Imaging, 413 East 69th Street, Suite 108, New York, New York 10021. E-mail: jkm2001@med. cornell.edu.

REFERENCES

1. Budoff MJ, Dowe D, Jollis JG, et al. Diagnostic performance of 64-multidetector row coronary computed tomographic angiography for evaluation of coronary artery stenosis in individuals without known coronary artery disease: results from the prospective multicenter ACCURACY (Assessment by Coronary Computed Tomographic Angiography of Individuals Undergoing Invasive Coronary Angiography) trial. J Am Coll Cardiol 2008;52:1724–32.

2. Miller JM, Rochitte CE, Dewey M, et al. Diagnostic performance of coronary angiography by 64-row CT. N Engl J Med 2008;359:2324–36.

3. Hounsfield GN. Computerized transverse axial scanning (tomography). 1. Description of system. Br J Radiol 1973;46:1016–22.

4. So A, Hsieh J, Narayanan S, et al. Dual-energy CT and its potential use for quantitative myocardial CT perfusion. J Cardiovasc Comput Tomogr 2012;6:308–17.

5. Wang R, Yu W, Wang Y, et al. Incremental value of dual-energy CT to coronary CT angiography for the detection of significant coronary stenosis: comparison with quantitative coronary angiography and single photon emission computed tomography. Int J Cardiovasc Imaging 2011;27:647–56.

6. Ko SM, Choi JW, Hwang HK, Song MG, Shin JK, Chee HK. Diagnostic performance of combined noninvasive anatomic and functional assessment with dual-source CT and adenosine-induced stress dual-energy CT for detection of significant coronary stenosis. AJR Am J Roentgenol 2012;198:512–20.

7. Blankstein R, Shturman LD, Rogers IS, et al. Adenosine-induced stress myocardial perfusion imaging using dual-source cardiac computed tomography. J Am Coll Cardiol 2009;54:1072–84.

8. Meyer M, Nance JW Jr., Schoepf UJ, et al. Cost-effectiveness of substituting dual-energy CT for SPECT in the assessment of myocardial perfusion for the workup of coronary artery disease. Eur J Radiol 2012;81:3719–25.

9. Ko SM, Choi JW, Song MG, et al. Myocardial perfusion imaging using adenosine-induced stress dual-energy computed tomography of the heart: comparison with cardiac magnetic resonance imaging and conventional coronary angiography. Eur Radiol 2011;21:26–35.

10. Wang Y, Qin L, Shi X, et al. Adenosine-stress dynamic myocardial perfusion imaging with second-generation dual-source CT: comparison with conventional catheter coronary angiography and SPECT nuclear myocardial perfusion imaging. AJR Am J Roentgenol 2012;198:521–9.

11. Ruzsics B, Schwarz F, Schoepf UJ, et al. Comparison of dual-energy computed tomography of the heart with single photon emission computed tomography for assessment of coronary artery stenosis and of the myocardial blood supply. Am J Cardiol 2009;104:318–26.

12. Weininger M, Schoepf UJ, Ramachandra A, et al. Adenosine-stress dynamic real-time myocardial perfusion CT and adenosine-stress first-pass dual-energy myocardial perfusion CT for the assessment of acute chest pain: initial results. Eur J Radiol 2012;81:3703–10.

13. Danad I, Raijmakers PG, Appelman YE, et al. Quantitative relationship between coronary artery calcium score and hyperemic myocardial blood flow as assessed by hybrid 15O-water PET/CT imaging in patients evaluated for coronary artery disease. J Nucl Cardiol 2012;19:256–64.

14. Ko SM, Park JH, Hwang HK, Song MG. Direct comparison of stress- and rest-dual-energy computed tomography for detection of myocardial perfusion defect. Int J Cardiovasc Imaging 2014;30 Suppl 1:41–53.

15. Danad I, Raijmakers PG, Knaapen P. Diagnosing coronary artery disease with hybrid PET/CT: it takes two to tango. J Nucl Cardiol 2013;20:874–90.

16. Carrascosa PM, Deviggiano A, Capunay C, et al. Incremental value of myocardial perfusion over coronary angiography by spectral computed tomography in patients with intermediate to high likelihood of coronary artery disease. Eur J Radiol 2015;84:637–42.

17. Meinel FG, De Cecco CN, Schoepf UJ, et al. First-arterial-pass dual-energy CT for assessment of myocardial blood supply: do we need rest, stress, and delayed acquisition? Comparison with SPECT. Radiology 2014;270:708–16.

18. Finn AV, Nakano M, Narula J, Kolodgie FD, Virmani R. Concept of vulnerable/unstable plaque. Arterioscler Thromb Vasc Biol 2010;30:1282–92.

19. Naghavi M, Libby P, Falk E, et al. From vulnerable plaque to vulnerable patient: a call for new definitions and risk assessment strategies: part II. Circulation 2003;108:1772–8.

20. Naghavi M, Libby P, Falk E, et al. From vulnerable plaque to vulnerable patient: a call for new definitions and risk assessment strategies: part I. Circulation 2003;108:1664–72.

21. Petranovic M, Soni A, Bezzera H, et al. Assessment of nonstenotic coronary lesions by 64-slice multidetector computed tomography in comparison to intravascular ultrasound: evaluation of nonculprit coronary lesions. J Cardiovasc Comput Tomogr 2009;3:24–31.

22. Leber AW, Knez A, Becker A, et al. Accuracy of multidetector spiral computed tomography in identifying and differentiating the composition of coronary atherosclerotic plaques: a comparative study with intracoronary ultrasound. J Am Coll Cardiol 2004;43:1241–7.

23. Pohle K, Achenbach S, Macneill B, et al. Characterization of non-calcified coronary atherosclerotic plaque by multi-detector row CT: comparison to IVUS. Atherosclerosis 2007;190:174–80.

24. Tanami Y, Ikeda E, Jinzaki M, et al. Computed tomographic attenuation value of coronary atherosclerotic plaques with different tube voltage: an ex vivo study. J Comput Assist Tomogr 2010;34:58–63.

25. Obaid DR, Calvert PA, Gopalan D, et al. Dual-energy computed tomography imaging to determine atherosclerotic plaque composition: a prospective study with tissue validation. J Cardiovasc Comput Tomogr 2014;8:230–7.

26. Henzler T, Porubsky S, Kayed H, et al. Attenuation-based characterization of coronary atherosclerotic plaque: comparison of dual source and dual energy CT with single-source CT and histopathology. Eur J Radiol 2011;80:54–9.

27. Scheffel H, Alkadhi H, Plass A, et al. Accuracy of dual-source CT coronary angiography: first experience in a high pre-test probability population without heart rate control. Eur Radiol 2006;16:2739–47.

28. Sun G, Li M, Jiang ZW, et al. Diagnostic accuracy of dual-source CT coronary angiography in patients with atrial fibrillation: meta analysis. Eur J Radiol 2013;82:1749–54.

29. Scheske JA, O'Brien JM, Earls JP, et al. Coronary artery imaging with single-source rapid kilovolt peak-switching dual-energy CT. Radiology 2013;268:702–9.

30. Yu L, Christner JA, Leng S, Wang J, Fletcher JG, McCollough CH. Virtual monochromatic imaging in dual-source dual-energy CT: radiation dose and image quality. Med Phys 2011;38:6371–9.

31. So A, Hsieh J, Imai Y, et al. Prospectively ECG-triggered rapid kV-switching dual-energy CT for quantitative imaging of myocardial perfusion. J Am Coll Cardiol Img 2012;5:829–36.

32. Bamberg F, Dierks A, Nikolaou K, Reiser MF, Becker CR, Johnson TR. Metal artifact reduction by dual energy computed tomography using monoenergetic extrapolation. Eur Radiol 2011;21:1424–9.

33. Boll DT, Merkle EM, Paulson EK, Fleiter TR. Coronary stent patency: dual-energy multidetector CT assessment in a pilot study with anthropomorphic phantom. Radiology 2008;247:687–95.

34. Boll DT, Merkle EM, Paulson EK, Mirza RA, Fleiter TR. Calcified vascular plaque specimens: assessment with cardiac dual-energy multidetector CT in anthropomorphically moving heart phantom. Radiology 2008;249:119–26.

35. Stehli J, Fuchs TA, Singer A, et al. First experience with single-source, dual-energy CCTA for monochromatic stent imaging. Eur Heart J Cardiovasc Imaging 2015;16:507–12.

36. Secchi F, De Cecco CN, Spearman JV, et al. Monoenergetic extrapolation of cardiac dual energy CT for artifact reduction. Acta Radiol 2015;56:413–8.

37. Yamada M, Jinzaki M, Kuribayashi S, Imanishi N, Funato K, Aiso S. Beam-hardening correction for virtual monochromatic imaging of myocardial perfusion via fast-switching dual-kVp 64-slice computed tomography: a pilot study using a human heart specimen. Circ J 2012;76:1799–801.

38. So A, Lee TY, Imai Y, et al. Quantitative myocardial perfusion imaging using rapid kVp

switch dual-energy CT: preliminary experience. J Cardiovasc Comput Tomogr 2011;5:430–42.

39. So A, Lee TY. Quantitative myocardial CT perfusion: a pictorial review and the current state of technology development. J Cardiovasc Comput Tomogr 2011;5:467–81.

40. Matsumoto K, Jinzaki M, Tanami Y, Ueno A, Yamada M, Kuribayashi S. Virtual monochromatic spectral imaging with fast kilovoltage switching: improved image quality as compared with that obtained with conventional 120-kVp CT. Radiology 2011;259:257–62.

41. Leipsic J, LaBounty TM, Mancini GB, et al. A prospective randomized controlled trial to assess the diagnostic performance of reduced tube voltage for coronary CT angiography. AJR Am J Roentgenol 2011;196:801–6.

42. Menke J, Unterberg-Buchwald C, Staab W, Sohns JM, Seif Amir Hosseini A, Schwarz A. Head-to-head comparison of prospectively triggered vs retrospectively gated coronary computed tomography angiography: meta-analysis of diagnostic accuracy, image quality, and radiation dose. Am Heart J 2013;165:154–63.e3.

43. Sun Z, Ng KH. Prospective versus retrospective ECG-gated multislice CT coronary angiography: a systematic review of radiation dose and diagnostic accuracy. Eur J Radiol 2012;81: e94–100.

44. Hausleiter J, Meyer T, Hadamitzky M, et al. Radiation dose estimates from cardiac multi-slice computed tomography in daily practice: impact of different scanning protocols on effective dose estimates. Circulation 2006;113: 1305–10.

45. Kerl JM, Bauer RW, Maurer TB, et al. Dose levels at coronary CT angiography—a comparison of dual energy-, dual source- and 16-slice CT. Eur Radiol 2011;21:530–7.

46. Halliburton SS, Sola S, Kuzmiak SA, et al. Effect of dual-source cardiac computed tomography on patient radiation dose in a clinical setting: comparison to single-source imaging. J Cardiovasc Comput Tomogr 2008;2:392–400.

47. Raju R, Thompson AG, Lee K, et al. Reduced iodine load with CT coronary angiography using dual-energy imaging: a prospective randomized trial compared with standard coronary CT angiography. J Cardiovasc Comput Tomogr 2014;8: 282–8.

48. Achenbach S, Marwan M, Schepis T, et al. High-pitch spiral acquisition: a new scan mode for coronary CT angiography. J Cardiovasc Comput Tomogr 2009;3:117–21.

49. Lell M, Marwan M, Schepis T, et al. Prospectively ECG-triggered high-pitch spiral acquisition for coronary CT angiography using dual source CT: technique and initial experience. Eur Radiol 2009; 19:2576–83.

50. Achenbach S, Goroll T, Seltmann M, et al. Detection of coronary artery stenoses by low-dose, prospectively ECG-triggered, high-pitch spiral coronary CT angiography. J Am Coll Cardiol Img 2011;4:328–37.

51. Achenbach S, Marwan M, Ropers D, et al. Coronary computed tomography angiography with

a consistent dose below 1 mSv using prospectively electrocardiogram-triggered high-pitch spiral acquisition. Eur Heart J 2010;31:340–6.

52. Alkadhi H, Stolzmann P, Desbiolles L, et al. Low-dose, 128-slice, dual-source CT coronary angiography: accuracy and radiation dose of the high-pitch and the step-and-shoot mode. Heart 2010;96:933–8.

53. Gordic S, Husarik DB, Desbiolles L, Leschka S, Frauenfelder T, Alkadhi H. High-pitch coronary CT angiography with third generation dual-source CT: limits of heart rate. Int J Cardiovasc Imaging 2014; 30:1173–9.

54. Hell MM, Bittner D, Schuhbaeck A, et al. Prospectively ECG-triggered high-pitch coronary angiography with third-generation dual-source CT at 70 kVp tube voltage: feasibility, image quality, radiation dose, and effect of iterative recon-struction. J Cardiovasc Comput Tomogr 2014;8: 418–25.

55. Leschka S, Stolzmann P, Desbiolles L, et al. Diagnostic accuracy of high-pitch dual-source CT for the assessment of coronary stenoses: first experience. Eur Radiol 2009;19:2896–903.

56. Morsbach F, Gordic S, Desbiolles L, et al. Performance of turbo high-pitch dual-source CT for coronary CT angiography: first ex vivo and patient experience. Eur Radiol 2014;24: 1889–95.

57. Schuhbaeck A, Achenbach S, Layritz C, et al. Image quality of ultra-low radiation exposure coronary CT angiography with an effective dose <0.1 mSv using high-pitch spiral acquisition and raw data-based iterative reconstruction. Eur Radiol 2013;23:597–606.

58. Yin WH, Lu B, Li N, et al. Iterative recon-struction to preserve image quality and diagnostic accuracy at reduced radiation dose in coronary CT angiography: an intraindividual comparison. J Am Coll Cardiol Img 2013;6:1239–49.

59. Yin WH, Lu B, Hou ZH, et al. Detection of coronary artery stenosis with sub-milliSievert radiation dose by prospectively ECG-triggered high-pitch spiral CT angiography and iterative reconstruction. Eur Radiol 2013;23:2927–33.

60. Numburi UD, Schoenhagen P, Flamm SD, et al. Feasibility of dual-energy CT in the arterial phase: imaging after endovascular aortic repair. AJR Am J Roentgenol 2010;195:486–93.

61. Kaufmann S, Sauter A, Spira D, et al. Tin-filter enhanced dual-energy-CT: image quality and accuracy of CT numbers in virtual noncontrast imaging. Acad Radiol 2013;20:596–603.

62. Yamada Y, Jinzaki M, Okamura T, et al. Feasi-bility of coronary artery calcium scoring on virtual unenhanced images derived from single-source fast kVp-switching dual-energy coronary CT angiography. J Cardiovasc Comput Tomogr 2014; 8:391–400.

63. Fuchs TA, Stehli J, Dougoud S, et al. Coronary artery calcium quantification from contrast en-hanced CT using gemstone spectral imaging and material decomposition. Int J Cardiovasc Imaging 2014;30:1399–405.

64. Moos SI, van Vemde DN, Stoker J, Bipat S. Contrast induced nephropathy in patients

undergoing intravenous (IV) contrast enhanced computed tomography (CECT) and the relationship with risk factors: a meta-analysis. Eur J Radiol 2013; 82:e387–99.

65. Yamamuro M, Tadamura E, Kanao S, et al. Coronary angiography by 64-detector row computed tomography using low dose of contrast material with saline chaser: influence of total in-jection volume on vessel attenuation. J Comput Assist Tomogr 2007;31:272–80.

66. Dilmanian FA, Wu XY, Parsons EC, et al. Single-and dual-energy CT with monochromatic synchrotron x-rays. Phys Med Biol 1997;42: 371–87.

67. Grant KL, Flohr TG, Krauss B, Sedlmair M, Thomas C, Schmidt B. Assessment of an advanced image-based technique to calculate virtual mon-oenergetic computed tomographic images from a dual-energy examination to improve contrast-to-noise ratio in examinations using iodinated contrast media. Invest Radiol 2014;49:586–92.

68. Carrascosa P, Capunay C, Rodriguez-Granillo GA, Deviggiano A, Vallejos J, Leipsic JA. Substantial iodine volume load reduction in CT angiography with dual-energy imaging: insights from a pilot randomized study. Int J Cardiovasc Imaging 2014;30:1613–20.

69. Cormode DP, Naha PC, Fayad ZA. Nanoparticle contrast agents for computed tomography: a focus on micelles. Contrast Media Mol Imaging 2014;9:37–52.

70. Peer D, Karp JM, Hong S, Farokhzad OC, Margalit R, Langer R. Nanocarriers as an emerging platform for cancer therapy. Nat Nanotechnol 2007;2:751–60.

71. van Schooneveld MM, Cormode DP, Koole R, et al. A fluorescent, paramagnetic and PEGylated gold/silica nanoparticle for MRI, CT and fluores-cence imaging. Contrast Media Mol Imaging 2010; 5:231–6.

72. Torchilin VP, Frank-Kamenetsky MD, Wolf GL. CT visualization of blood pool in rats by using long-circulating, iodine-containing micelles. Acad Radiol 1999;6:61–5.

73. Trubetskoy VS, Gazelle GS, Wolf GL, Torchilin VP. Block-copolymer of polyethylene glycol and polylysine as a carrier of organic iodine: design of long-circulating particulate contrast medium for X-ray computed tomography. J Drug Target 1997;4:381–8.

74. Kinsella JM, Jimenez RE, Karmali PP, et al. X-ray computed tomography imaging of breast cancer by using targeted peptide-labeled bismuth sulfide nanoparticles. Angew Chem Int Ed Engl 2011;50:12308–11.

75. Cormode DP, Roessl E, Thran A, et al. Atherosclerotic plaque composition: analysis with multicolor CT and targeted gold nanoparticles. Radiology 2010;256:774–82.

76. Cormode DP, Skajaa T, van Schooneveld MM, et al. Nanocrystal core high-density lipoproteins: a multimodality contrast agent platform. Nano Lett 2008;8:3715–23.

77. Hyafil F, Cornily JC, Feig JE, et al. Noninvasive detection of macrophages using a nanoparticulate

contrast agent for computed tomography. Nat Med 2007;13:636–41.

78. Hyafil F, Cornily JC, Rudd JH, Machac J, Feldman LJ, Fayad ZA. Quantification of inflammation within rabbit atherosclerotic plaques using the macrophage-specific CT contrast agent N1177: a comparison with 18F-FDG PET/CT and histology. J Nucl Med 2009;50:959–65.

79. Rabin O, Manuel Perez J, Grimm J, Wojtkiewicz G, Weissleder R. An X-ray computed tomography imaging agent based on long-circulating bismuth sulphide nanoparticles. Nat Mater 2006;5:118–22.

80. Pan D, Schirra CO, Senpan A, et al. An early investigation of ytterbium nanocolloids for selective and quantitative "multicolor" spectral CT imaging. ACS Nano 2012;6:3364–70.

81. Schlomka JP, Roessl E, Dorscheid R, et al. Experimental feasibility of multi-energy photon-counting K-edge imaging in pre-clinical computed tomography. Phys Med Biol 2008;53:4031–47.

82. Ronaldson JP, Zainon R, Scott NJ, et al. Toward quantifying the composition of soft tissues by spectral CT with Medipix3. Med Phys 2012;39:6847–57.

83. He P, Yu H, Thayer P, et al. Preliminary experimental results from a MARS Micro-CT system. J X-Ray Sci Technol 2012;20:199–211.

84. Iwanczyk JS, Nygard E, Meirav O, et al. Photon counting energy dispersive detector arrays for x-ray imaging. IEEE Trans Nucl Sci 2009;56:535–42.

85. Kappler S, Hannemann T, Kraft E, et al. First results from a hybrid prototype CT scanner for exploring benefits of quantum-counting in clinical CT. Proc SPIE 2012;8313.

86. Taguchi K, Iwanczyk JS. Vision 20/20: single photon counting x-ray detectors in medical imaging. Med Phys 2013;40:100901.

87. Feuerlein S, Roessl E, Proksa R, et al. Multi-energy photon-counting K-edge imaging: potential for improved luminal depiction in vascular imaging. Radiology 2008;249:1010–6.

88. Boussel L, Coulon P, Thran A, et al. Photon counting spectral CT component analysis of coronary artery atherosclerotic plaque samples. Br J Radiol 2014;87:20130798.

KEY WORDS dual-energy CT, molecular CT imaging, spectral CT